

Inorganic Acid-Impregnated Covalent Organic Gels as High-Performance Proton-Conductive Materials at Subzero Temperatures

Hong Zhong, Zhihua Fu, Jared M. Taylor, Gang Xu,* and Ruihu Wang*

Proton exchange membrane fuel cells usually suffer from severe power loss and even damage under subzero-temperature working surroundings, which restricts their practical use in cold climates and in high-altitude drones. One of the effective solutions to these issues is to develop new types of proton-conductive materials at subzero temperature. This study presents a series of acylhydrazone-based covalent organic gels (COGs). The COGs are stable in acidic media and show high proton conductivity over the temperature range of -40 to 60 °C under anhydrous conditions. Compared with other reported organic conductive materials, both a state-of-the-art conductivity of $3.8 \times 10^{-4} \text{ S cm}^{-1}$ at -40 °C and superior long-term stability are demonstrated. Moreover, the COGs possess remarkable self-sustainability, good processability, and superior mechanical properties, and may be processed and molded into any desirable shapes for practical applications. These advantages make COGs hold great promises as solid-state electrolytes under subzero-temperature operating conditions.

1. Introduction

Proton exchange membrane (PEM) fuel cells have captured intensive interest in electric vehicles, portable electronic devices, and smart grids.^[1] Proton-conductive materials are considered as one of the key components in PEM systems. Commercial Nafion-based electrolytes can reach proton conductivities of 10^{-1} – $10^{-2} \text{ S cm}^{-1}$ under highly relative humidity (98% RH) and moderate temperatures (60 – 80 °C), but some inherent problems, such as high cost, strong humidity dependence, and freezing damage caused by freeze/thaw cycles, have spurred researchers to develop alternatives in various working surroundings.^[2–4] Considerable efforts have been devoted to porous materials, such as mesoporous silica,^[3] metal–organic

frameworks (MOFs)^[4] and porous organic materials,^[5–8] for encapsulating proton-conductive media to form solid-state electrolytes, but most studies have focused on the operating conditions at high humidity and/or at temperatures above 100 °C. Although a handful of low-temperature porous conductive electrolytes have been reported,^[8,9] their poor conductivity at subzero temperatures greatly depresses their practical application in low-temperature environments, such as electric vehicles in cold climates and in high-altitude drones.^[10]

Among porous organic materials, covalent organic frameworks (COFs)^[6,7] and porous organic polymers (POPs)^[8] have gained increasing attention recently as new types of proton-conductive materials. They usually possess stable structures, flexible synthetic strategies, high surface

areas, and tunable pore sizes, which provide great potential to accommodate various aromatic heterocycles and nonvolatile strong acids into their inherent pores. In comparison with COFs and POPs, covalent organic gels (COGs) are very similar type of organic materials, and possess features as promising subzero-temperature electrolytes. COGs are generated inductively as intermediate aggregates in the polymerization of organic building blocks with multiple reactive groups.^[11] Their hierarchical porosity is desirable for incorporation of a broad variety of proton carriers, facile uptake of guest molecules, and rapid mass transport. These characteristics may significantly improve the mobility and concentration of proton carriers in the gel networks to achieve high proton conductivity. Moreover, most reported porous materials, such as MOFs, COFs, and POPs, can only be miniaturized to the particles size less than millimeters.^[12] These materials are normally unable to be melted or dissolved, which makes them difficult to be processed. Compressing these materials into pellets would inevitably generate a large amount of pin-hole defects, which induces gas penetration from one side of PEM to other side, thus significantly deteriorating the performances of the devices. Advantageously, COGs may be prepared into the bulk with required sizes and processed into any shapes without pin-hole defects for practical applications. Despite COGs possess these encouraging advantages, to the best of our knowledge, its proton conductivity is still unexplored.

Dr. H. Zhong, Dr. Z. H. Fu, Prof. G. Xu, Prof. R. H. Wang
State Key Laboratory of Structural Chemistry
Fujian Institute of Research on the Structure of Matter
Chinese Academy of Sciences
Fuzhou 350002, China
E-mail: gxu@fjirsm.ac.cn; ruihu@fjirsm.ac.cn

Prof. J. M. Taylor
Department of Chemistry
University of Calgary
Calgary, Alberta T2N 1N4, Canada

DOI: 10.1002/adfm.201701465

Herein, we report an acylhydrazone-based COG (COG-1), and present the first study of COGs as a new type of high-performance proton-conductive material down to temperature as low as $-40\text{ }^{\circ}\text{C}$. COG-1 can encapsulate different amounts of H_3PO_4 (PA) during the gelation to further improve its proton conductivity. The resultant COGs possess high proton conductivities and excellent long-term stability. In comparison with the reported conductive materials, such as MOFs, COFs, and POPs, the state-of-the-art conductivity at $-40\text{ }^{\circ}\text{C}$ and 1–3 orders of magnitude higher conductivity at $60\text{ }^{\circ}\text{C}$ have been demonstrated. Moreover, no detectable phase change occurs during their freeze/thaw cycles.

2. Results and Discussion

COG-1 was readily prepared by an imine bond formation reaction between benzene-1,3,5-tricarbohydrazide and 1,4-phthalaldehyde (Figure 1a). During the gelation, an emulsion was formed instantly from a translucent solution of the starting materials in the presence of hydrochloric acid in *N,N*-dimethylformamide (DMF) (Figure S1a–e, Supporting Information). Subsequent heating at $80\text{ }^{\circ}\text{C}$ for 72 h generated a pale-yellow opaque gel (Figure S1f, Supporting Information). The gel had no obvious change after either further heating at $80\text{ }^{\circ}\text{C}$ for 1 week (Figure S1g, Supporting Information) or freezing at $-40\text{ }^{\circ}\text{C}$ overnight (Figure S1h, Supporting Information), suggesting that the gelation process is thermo-irreversible. Strikingly, the addition of 1, 5, and 10 equivalent of PA with respect to imine group had no detectable effect on the gelation process

(Figure S2, Supporting Information). The resultant gels were denoted as COG-1P, COG-5P, and COG-10P, respectively.

In order to characterize COGs in detail, the model molecule *N,N',N''*-(tribenzylidene)benzene-1,3,5-tricarbohydrazide (TBCH, Figure S3, Supporting Information) and the xerogel of COG-1 (COG-xerogel) were prepared. In the Fourier transform infrared (FTIR) spectra of the COGs and COG-xerogel, the characteristic peaks of the host backbones are identical with that of TBCH (Figure 1b). The peaks of the C=N stretching vibrations occur at 1550 and 1258 cm^{-1} , while the peak at 1670 cm^{-1} corresponds to the stretching vibration of C=O.^[13] In comparison with the characteristic peak of C=O at 1694 cm^{-1} for 1,4-phthalaldehyde and at 1652 cm^{-1} for benzene-1,3,5-tricarbohydrazide, the corresponding red shift of 24 cm^{-1} and blueshift of 18 cm^{-1} in COG-1 are attributed to a strength variation of C=O bond as a result of resonance with the imine. It is also noteworthy that no signal for the stretching vibrations of the aldehyde group is observed in FTIR spectra of both the COGs and COG-xerogel, indicating the total consumption of the starting materials. Solid-state ^{13}C NMR spectrum of the COG-xerogel provides further evidence of acylhydrazone linkage (Figure S4a, Supporting Information), the peaks at 161 and 149 ppm are assigned as the carbon atoms of C=O and C=N bonds, respectively, which are associated with that in ^{13}C NMR spectrum of TBCH (Figure S4b, Supporting Information). Scanning electron microscopy (SEM) and transmission electron microscope images reveal the porosity of COGs (Figures S5 and S6, Supporting Information). The nitrogen isotherm at 77 K of COG-xerogel exhibits a type IV adsorption branch (Figure S7, Supporting Information). Powder X-ray diffraction patterns of COGs and COG-xerogel

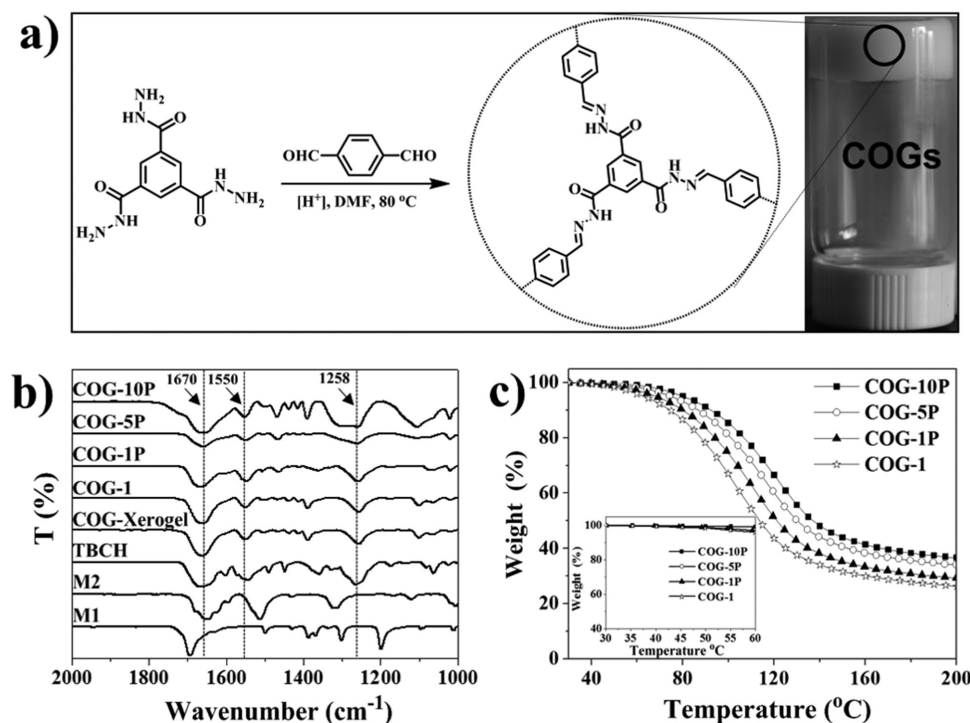


Figure 1. a) Schematic illustration for the synthesis of COGs; b) FTIR spectra for 1,4-phthalaldehyde (M1), benzene-1,3,5-tricarbohydrazide (M2), TBCH, COGs, and COG-xerogel; c) TGA curves for COGs in the temperature range of 30–200 °C and 30–60 °C (inset).

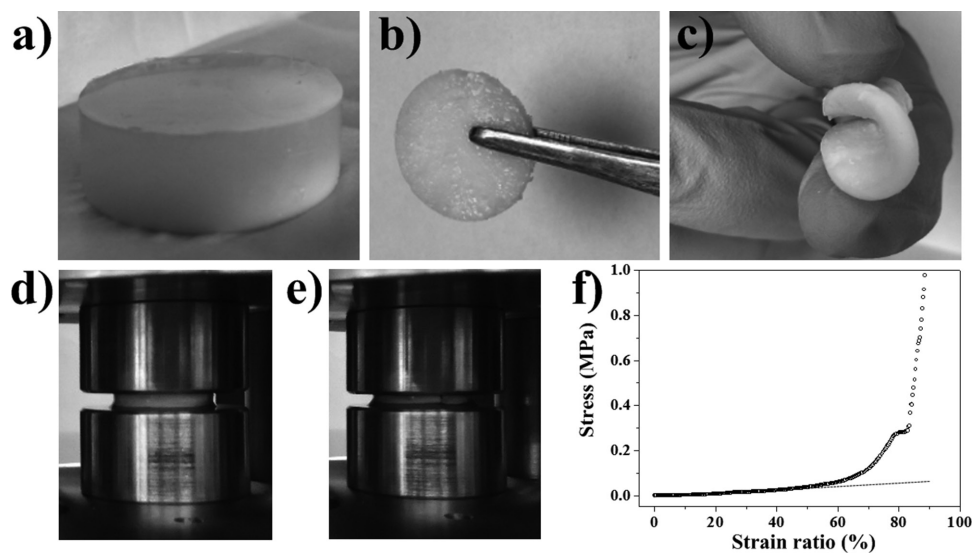


Figure 2. Self-sustaining and processable behavior of COG-1: a) COG-1 was removed from the synthesis vial; b) COG-1 was tailored into a slice; c) the slice was bent into high curvature; Stress–strain experiments of COG-1 d) before compression and e) at the moment for crack appearance; f) Stress–strain curve of COG-1.

reveal that they are amorphous (Figure S8, Supporting Information), which is common for gel materials.^[11]

All of COGs possess outstanding stability in an acidic medium, and show excellent self-sustainability. As shown in **Figure 2a**, COG-1 can retain its original shape after it was taken out from the synthesis vial. Compared with reported MOFs, COFs, and POPs, COGs show great advantages in the processability. They can be easily tailored into required shapes or slices (Figure 2a; and Figure S9, Supporting Information). The slice has good flexibility and it can be bent from flat to high curvature (Figure 2b,c). Notably, the thin membrane with a thickness of 2.4 μm can be also obtained, it has good mechanical properties and can be folded more than 100 times (Figure S10, Supporting Information), indicating these materials may be directly used as a solid-state electrolyte in fuel cell devices. COG-1 was further analyzed by stress–strain experiments, it can keep intact structure before compressed to a strain ratio of 45% upon a small stress of 0.032 MPa (Figure 2d–f). When the compressive stress was more than 0.285 MPa, an obvious crack on the gel appeared with a strain ratio over 55%. COG-1 was completely destroyed with a strain ratio up to 80%. SEM images show the morphology of the compressed COG-1 has no obvious change before the gel starts to crack, but it is totally changed after COG-1 is completely destroyed (Figure S11, Supporting Information).

In thermogravimetric analysis (TGA) curves of COG-1, COG-1P, COG-5P, and COG-10P (Figure 1c), there is no obvious weight loss before 60 $^{\circ}\text{C}$. The first weight losses of 45–62% occur between 60 and 130 $^{\circ}\text{C}$, which correspond to the removal of trapped guest molecules, while COG-xerogel shows a negligible weight loss before 130 $^{\circ}\text{C}$ and is stable up to 280 $^{\circ}\text{C}$, which is close to that of TBCH (Figure S12, Supporting Information). Elemental analysis results of COG-xerogel show that the experimental values of C and N are lower than respective theoretical values, which is probably attributed to incomplete removal of trapped guest molecules owing to the presence of

extensive hydrogen bonds. However, the N/C molar ratio of 0.34 in COG-xerogel is very close to the theoretical value of 0.33. Differential scanning calorimetry analyses indicate that there is no detectable phase transition between –40 and 40 $^{\circ}\text{C}$ in the COGs (Figure S13, Supporting Information). These features demonstrate that the COGs can be promising proton-conductive materials at subzero temperatures, the contraction and expansion caused by phase change of proton-conductive media are negligible for COGs.

The anhydrous proton conductivities of the COGs were measured with a quasi-four-probe alternating current impedance technique by sealing the samples in quartz tubes (Table S1, Supporting Information). The typical Nyquist plots of COGs in the temperature range of –40 to 60 $^{\circ}\text{C}$ are shown in **Figure 3a,b**, and Figures S14 and S15, Supporting Information. The plots are characterized by a single arc in the high-frequency region, which is similar to the observations in the reported proton-conductive materials.^[14] The resistance values were obtained by fitting the Nyquist plots based on the equivalent circuits (Figure S16, Supporting Information). The diameter of the arc decreases with the rise of temperature, suggesting the increment of the conductivity. COG-1 has a proton conductivity of $1.8 \times 10^{-4} \text{ S cm}^{-1}$ at –40 $^{\circ}\text{C}$ (Figure S17a, Supporting Information). The introduction of PA into COG-1 further enhances its proton conductivity at subzero temperatures. When PA loading is increased from 1 to 10 equivalents, the conductivity of the material rises accordingly and reaches the highest value of $3.8 \times 10^{-4} \text{ S cm}^{-1}$ at –40 $^{\circ}\text{C}$ (Figure S17b, Supporting Information). The enhanced conductivity is attributed that higher ratio of PA imparts higher concentration of mobile protons and forms a more extensive hydrogen-bond network for facile proton movement. Notably, there are few reported materials possessing proton-conductive properties at subzero temperatures.^[15] COGs not only represent a new type of solid state proton-conductive material, but also show the state-of-the-art conductivity at –40 $^{\circ}\text{C}$ compared to other porous materials

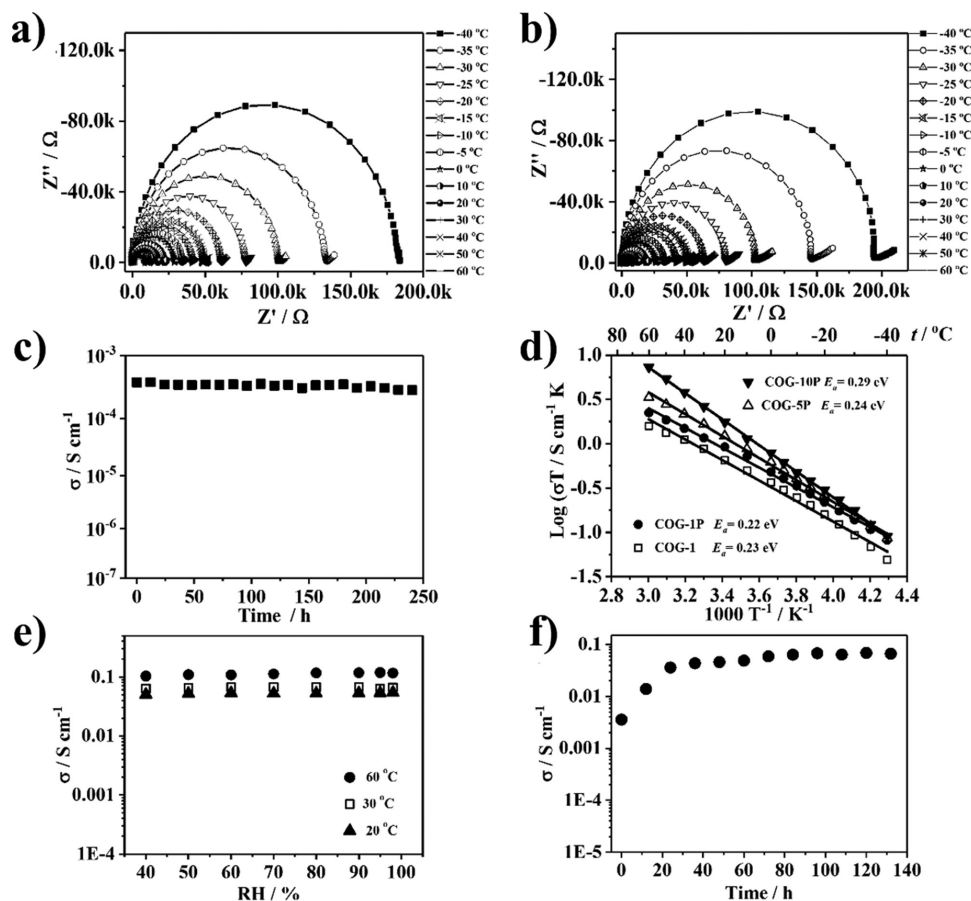


Figure 3. Typical Nyquist plots at different temperatures for a) COG-1 and b) COG-10P; c) long-term stability measurement at $-40\text{ }^{\circ}\text{C}$ for COG-10P; d) variable temperature conductivities of COGs showing linear Arrhenius behavior; e) The humidity-dependent conductivities of COG-10P at different temperature; f) long-term stability measurement under 98% RH at $30\text{ }^{\circ}\text{C}$ for COG-10P.

impregnated with PA, hydrochloric acid, imidazole, hydroquinone, or cyclohexanol (Figure 4).^[15–18] COG-10P also shows excellent long-term stability at low temperatures. As shown in

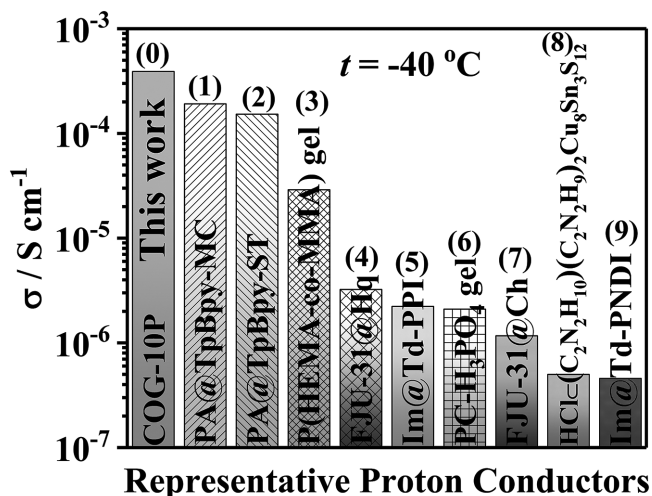


Figure 4. The comparison of proton conductivity POG-10P with representative porous proton-conductors at $-40\text{ }^{\circ}\text{C}$. (1)–(9) refer to refs. [8,16,17,18a–c].

Figure 3c, its conductivity has little variation after consecutive cycles at $-40\text{ }^{\circ}\text{C}$ for at least 10 d. The high conductivity and superior stability of the COGs at subzero temperatures endow them with the potential to work as PEMs for fuel cells in on-board automotive application, which require better materials for subzero temperature start-up in cold climates.^[19]

The COGs exhibit remarkable proton conductivity in a wide temperature range under anhydrous conditions. The conductivities of the COGs enhance by more than 1 order of magnitude by increasing the temperature from -40 to $60\text{ }^{\circ}\text{C}$ (Figures S14–S16, Supporting Information). COG-10P shows the highest conductivity among these COGs, and its conductivity at $60\text{ }^{\circ}\text{C}$ reaches $2.3 \times 10^{-2}\text{ S cm}^{-1}$, which is 1–3 orders of magnitude higher than those in reported H_2SO_4 - and PA-loaded porous materials ($\approx 2.3 \times 10^{-5}$ – $1.45 \times 10^{-3}\text{ S cm}^{-1}$).^[6,16,20,21]

The plots of temperature-dependent conductivity of COGs under anhydrous conditions show linear Arrhenius behavior (Figure 3d), further indicating they are thermally stable in the temperature range of -40 to $60\text{ }^{\circ}\text{C}$, and there is no apparent phase change during the heating process. The proton conductivities in the heating-cooling cycles were also measured (Figure S18, Supporting Information). The curves of heating and cooling processes are almost identical, suggesting that the conductivity of COG-10P possesses good repeatability and stability

in a wide temperature range. The activation energies (E_a) for proton transport in the COGs were calculated using the Arrhenius equation.^[22] By the least-squares fits of the slopes, the derived E_a values of the COGs are relatively small and fall in the range of 0.22–0.29 eV, which are similar to those of Nafion (0.22 eV).^[23] According to these E_a values, the proton conduction of the COGs may be assigned to the Grothuss mechanism ($E_a = 0.1$ –0.4 eV). The high proton conductivities and low E_a in the COGs clearly suggest they are promising conductors for proton transportation at subzero temperatures.

Both COG-1 (Figure S19, Supporting Information) and COG-10P (Figure 3e) have constant proton-conductive properties under different RH. The conductivity of COG-10P only changes 8% at maximum upon changing RH from 40% to 98% at 20, 30, and 60 °C, respectively. Under 98% RH, COG-10P shows smooth increment of proton conductivity when varying temperature from 10 to 80 °C (Figure S20, Supporting Information). At 80 °C and 98% RH, COG-10 still keeps its colloidal state and affords a very high conductivity of 0.14 S cm⁻¹. This value is almost the same as that of Nafion 117 and is superior to those in most of reported gel materials under the same conditions (Table S2, Supporting Information). The active energy of COG-10P ($E_a = 0.18$ eV) at 98% RH is lower than that of COG-1 ($E_a = 0.21$ eV), which shows that PA doping in the COGs is beneficial to proton conduction. The activation energy is also lower than that under anhydrous conditions, suggesting the presence of water can further promote the proton conduction in the gel system. Although the conductivity of COG-10P under 98% RH at 30 °C gradually increases in the first 24 h due to slow adsorption of small amount of water under high RH,^[24,25] high conductivities are maintained subsequently for at least 6 d (Figure 3f), suggesting excellent stability of COG-10P under high humidity.

The proton conduction behavior of COG-10P was verified by sandwiching it between palladium/carbon electrodes (Figure 5). Under N₂ atmosphere, the current mainly originates from the depletion of protons in COG-10, which shows a rapid decrement of current when applied a direct current (DC) field. However, when switching to 5% H₂ atmosphere, the current of COG-10 enhances up to seven folds. The current increment is attributed to the formation of palladium hydride (PdH_x) to act as a source of proton on exposure to H₂.^[26] Under H₂ atmosphere, PdH_x electrodes continuously inject and drain H⁺ into and from the COG-10 to generate an enhanced proton flux current.^[27] These results clearly demonstrate the intrinsic proton conduction of COG-10P.

3. Conclusion

A new type of subzero-temperature proton-conductive materials has been presented. The outstanding stability toward

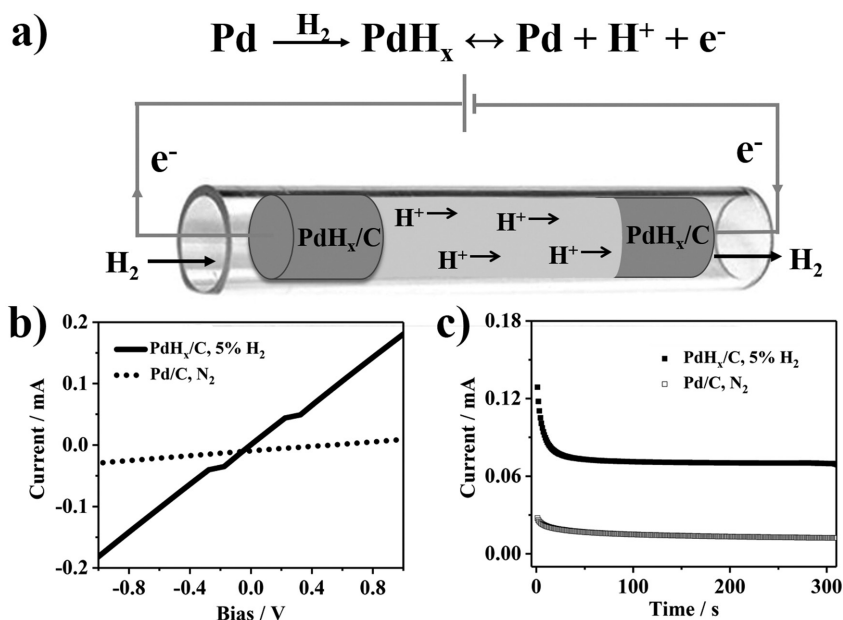


Figure 5. a) The schematic diagram of the setup for DC measurement; b) I - V curves for COG-10P under 5% H₂ and N₂; c) Transient responses of COG-10P to 1 V under N₂ and 5% H₂.

strong acid and hierarchical porosity enable COG-1 to encapsulate a plethora of inorganic acids, resulting in the improvement of mobile proton concentration to achieve high proton conductivity. These COGs not only possess remarkable self-sustaining nature and superior processability, but also show high conductivities and excellent long-term stability. The conductivity of COGs greatly outperforms those in other reported conductive materials, and even can compete with Nafion membranes. The encouraging performance of COGs provides a new inspiration for the development of subzero-temperature proton-conductive materials for practical applications in cold climates and high-altitude drones.

4. Experimental Section

Synthesis of *N,N',N''*-(Tribenzylidene)Benzene-1,3,5-Tricarbohydrazide: Benzene-1,3,5-tricarbohydrazide (25 mg, 0.10 mmol) and benzaldehyde (64 mg, 0.60 mmol) were dissolved in a mixture solvent of EtOH and H₂O (10 mL, v/v = 9:1). After aqueous hydrochloric acid (36 wt%, 25 μL) was added, the reaction mixture was kept at 60 °C for 48 h. The resulting solid was isolated by filtration, washed with EtOH, and dried in vacuo. Yield: 46 mg (90%). IR (KBr, cm⁻¹): 1670 (s), 1602 (m), 1545 (s), 1490 (m), 1448 (m), 1357 (m), 1266 (s), 1175 (w), 1064 (m), 959 (w), 757 (m), 728 (m), 692 (m), 511 (w).

Synthesis of COG-1: 1,4-Phthalaldehyde (33.5 mg, 0.250 mmol) in DMF (2 mL) was added to a DMF (2 mL) solution of benzene-1,3,5-tricarbohydrazide (42 mg, 0.167 mmol) with two drop of hydrochloric acid (0.5 mol L⁻¹ in DMF). The resulting mixture was heated at 80 °C for 72 h to give rise to COG-1 as a pale yellow gel.

Synthesis of COG-Xerogel: COG-1 gel was immersed in methanol (200 mL) at room temperature for 6 h, the process was repeated for four times with the replacement of methanol to exchange DMF from the gelation reaction. The resulting solid was further treated by Soxhlet extraction with dichloromethane overnight, and subsequent drying in vacuo at 80 °C for 12 h gave rise to COG-xerogel. Elemental analysis calculated (%) for C₇H₅N₂O: C, 63.16; H, 3.76; N, 21.05. Found: C,

54.43; H, 4.73; N, 18.68. IR (KBr cm^{-1}): 3452 (m), 3021 (m), 2772 (m), 1670 (s), 1610 (m), 1550 (s), 1466 (m), 1363 (m), 1259 (s), 1069 (m), 1020 (m), 954 (m), 830 (m).

Synthesis of COG-1P: COG-1P was prepared using similar method to COG-1 except that 1 equivalent of H_3PO_4 (46 μL , 85 wt% in water) with respect to imine was added in DMF solution of benzene-1,3,5-tricarbohydrazide.

Synthesis of COG-5P: COG-5P was prepared using similar method to COG-1 except that 5 equivalent of H_3PO_4 (230 μL , 85 wt% in water) with respect to imine was added in DMF solution of benzene-1,3,5-tricarbohydrazide.

Synthesis of COG-10P: COG-10P was prepared using similar method to COG-1 except that 10 equivalent of H_3PO_4 (460 μL , 85 wt% in water) with respect to imine was added in DMF solution of benzene-1,3,5-tricarbohydrazide.

Proton Conductivity Measurement: The proton conductivities of COGs were carried out with Solartron SI 1260 impedance/gain-phase analyzer using a quasi-four-probe method in the frequency range from 1 to 10 MHz at an AC amplitude of 200 mV. For each measurement, the gel sample was compressed into quartz tube with both ends of gold wires and gold paste. All the samples were carried out in the constant temperature and humidity equipment (XK-CTS80Z, 220 V, 3.5 kW). The samples were sealed by epoxy resin in tube to be tested in the anhydrous condition (from -40 to 60 $^{\circ}\text{C}$). The unsealed samples sandwiched by gold electrodes in the quartz tube were tested under different relative humidity (40–98% RH). Three temperature points (20, 30, and 60 $^{\circ}\text{C}$) were selected to measure the effect of humidity (from 40% to 98% RH). The stability testing was measured at the condition of 30 $^{\circ}\text{C}$, 98% RH. The proton conductivity values were calculated by using the equation $\sigma = L/RS$, L : length of sample, R : resistance, and S : cross-sectional area of sample.

Supporting Information

Supporting Information is available from the Wiley Online Library or from the author.

Acknowledgements

Hong Zhong and Zhihua Fu contributed equally to this work. The authors acknowledge National Natural Science Foundation of China (Nos. 21603228, 51402293, and 21273239) and Strategic Priority Research Program of the Chinese Academy of Sciences (No. XDB20000000) for financial support.

Conflict of Interest

The authors declare no conflict of interest.

Keywords

acylhydrazone, electrolyte, gels, proton conductivity, subzero temperature

Received: March 20, 2017
Revised: May 25, 2017
Published online: July 20, 2017

- [1] J. H. Wee, *Renewable Sustainable Energy Rev.* **2007**, *11*, 1720.
[2] a) G. K. Shimizu, J. M. Taylor, S. Kim, *Science* **2013**, *341*, 354; b) M. Yoon, K. Suh, S. Natarajan, K. Kim, *Angew. Chem. Int. Ed.* **2013**, *52*, 2688; c) S. Horike, D. Umeyama, S. Kitagawa, *Acc. Chem. Res.* **2013**, *46*, 2376.

- [3] C. Liang, J. Li, H. Tang, H. Zhang, P. Mu, *J. Mater. Chem. A* **2014**, *2*, 753.
[4] a) J. A. Hurd, R. Vaidhyanathan, V. Thangadurai, C. I. Ratcliffe, I. L. Moudrakovski, G. K. H. Shimizu, *Nat. Chem.* **2009**, *1*, 705; b) S. Bureekaew, S. Horike, M. Higuchi, M. Mizuno, T. Kawamura, D. Tanaka, N. Yanai, S. Kitagawa, *Nat. Mater.* **2009**, *8*, 831; c) M. Sadakiyo, T. Yamada, H. Kitagawa, *J. Am. Chem. Soc.* **2014**, *136*, 13166; d) W. Chen, S. Horike, D. Umeyama, N. Ogiwara, T. Itakura, C. Tassel, Y. Goto, H. Kageyama, S. Kitagawa, *Angew. Chem. Int. Ed.* **2016**, *55*, 5195; e) T. Kobayashi, T. Ichikawa, T. Kato, H. Ohno, *Adv. Mater.* **2017**, *29*, 1604429.
[5] a) D. Mecerreyes, H. Grande, O. Miguel, E. Ochoteco, R. Marcilla, I. Cantero, *Chem. Mater.* **2004**, *16*, 604; b) M. K. Song, H. Li, J. Li, D. Zhao, J. Wang, M. Liu, *Adv. Mater.* **2014**, *26*, 1277; c) H. Ma, B. Liu, B. Li, L. Zhang, Y. G. Li, H. Q. Tan, H. Y. Zang, G. J. Zhu, *Am. Chem. Soc.* **2016**, *138*, 5897.
[6] H. Xu, S. Tao, D. Jiang, *Nat. Mater.* **2016**, *15*, 722.
[7] S. Chandra, T. Kundu, S. Kandambeth, R. BabaRao, Y. Marathe, S. M. Kunjir, R. Banerjee, *J. Am. Chem. Soc.* **2014**, *136*, 6570.
[8] Y. Ye, L. Zhang, Q. Peng, G. Wang, Y. Shen, Z. Li, L. Wang, X. Ma, Q. H. Chen, Z. Zhang, S. Xiang, *J. Am. Chem. Soc.* **2015**, *137*, 913.
[9] P. Ramaswamy, N. E. Wong, G. K. H. Shimizu, *Chem. Soc. Rev.* **2014**, *43*, 5913.
[10] C. Zhang, G. Zhang, S. Ge, T. Xu, Y. Ji, X. Yang, Y. Leng, *Nature* **2016**, *529*, 515.
[11] a) S. Y. Moon, J. S. Bae, E. Jeon, J. W. Park, *Angew. Chem. Int. Ed.* **2010**, *49*, 9504; b) W. Luo, Y. Zhu, J. Zhang, J. He, Z. Chi, P. W. Miller, L. Chen, C. Y. Su, *Chem. Commun.* **2014**, *50*, 11942.
[12] a) H. X. Zhao, X. X. Li, L. Y. Li, R. H. Wang, *Small* **2015**, *11*, 3642; b) G. W. Zhan, H. C. Zeng, *Adv. Funct. Mater.* **2016**, *26*, 3268; c) R. Sakamoto, K. Takada, X. S. Sun, T. Pal, T. Tsukamoto, E. J. H. Phua, A. Rapakousiou, K. Hoshiko, H. Nishihara, *Coord. Chem. Rev.* **2016**, *320–321*, 118.
[13] a) F. J. Uribe-Romo, C. J. Doonan, H. Furukawa, K. Oisaki, O. M. Yaghi, *J. Am. Chem. Soc.* **2011**, *133*, 11478; b) G. Das, D. B. Shinde, S. Kandambeth, B. P. Biswal, R. Banerjee, *Chem. Commun.* **2014**, *50*, 12615; c) C. Zhang, G. Li, Z. Zhang, *J. Chromatogr. A* **2015**, *1*, 1419; d) Q. Yang, H. Cai, S. Yuan, X. Wang, W. Yuan, *Int. J. Hydrogen Energy* **2013**, *38*, 1016; e) J. Zhang, L. Liu, H. Liu, M. Lin, S. Li, G. Ouyang, L. Chen, C. Y. Su, *J. Mater. Chem. A* **2015**, *3*, 10990.
[14] a) D. Pergolesi, E. Fabbri, A. D'Epifanio, E. Di Bartolomeo, A. Tebano, S. Sanna, S. Licocchia, G. Balestrino, E. Traversa, *Nat. Mater.* **2010**, *9*, 846; b) G. Xu, K. Otsubo, T. Yamada, S. Sakaida, H. Kitagawa, *J. Am. Chem. Soc.* **2013**, *135*, 7438; c) Q. Tang, Y. Liu, S. Liu, D. He, J. Miao, X. Wang, G. Yang, Z. Shi, Z. Zheng, *J. Am. Chem. Soc.* **2014**, *136*, 12444; d) W. J. Phang, H. Jo, W. R. Lee, J. H. Song, K. Yoo, B. Kim, C. S. Hong, *Angew. Chem. Int. Ed.* **2015**, *54*, 5142; e) S. Bhadra, N. H. Kim, J. H. Lee, *J. Membr. Sci.* **2010**, *349*, 304; f) H. Pei, L. Hong, J. Y. Lee, *J. Membr. Sci.* **2008**, *307*, 126.
[15] a) S. Takamuku, P. Jannasch, *Adv. Energy Mater.* **2012**, *2*, 129; b) J. Hou, H. Yu, L. Wang, D. Xing, Z. Hou, P. Ming, Z. Shao, B. Yi, *J. Power Sources* **2008**, *180*, 232; c) S. Takamuku, P. Jannasch, *Polym. Chem.* **2012**, *3*, 1202.
[16] D. B. Shinde, H. B. Aiyappa, M. Bhadra, B. Biswal, P. Wadge, S. Kandambeth, B. Garai, T. Kundu, S. Kurungot, R. Banerjee, *J. Mater. Chem. A* **2016**, *4*, 2682.
[17] H. B. Luo, L. T. Ren, W. H. Ning, S. X. Liu, J. L. Liu, X. M. Ren, *Adv. Mater.* **2016**, *28*, 1663.
[18] a) Y. Ye, X. Wu, Z. Yao, L. Wu, Z. Cai, L. Wang, X. Ma, Q. H. Chen, Z. Zhang, S. Xiang, *J. Mater. Chem. A* **2016**, *4*, 4062; b) A. A. Łatoszyńska, G. Z. Żukowska, I. A. Rutkowska, P. L. Taberna, P. Simon, P. J. Kulesza, W. Wieczorek, *J. Power Sources* **2015**, *274*, 1147; c) D. Raducha, W. Wieczorek, Z. Florjanczyk, J. R. Stevens, *J. Phys. Chem.* **1996**, *100*, 20126.

- [19] Z. Wan, H. Chang, S. Shu, Y. Wang, H. Tang, *Energies* **2014**, *7*, 3179.
- [20] V. G. Ponomareva, K. A. Kovalenko, A. P. Chupakhin, D. N. Dybtsev, E. S. Shutova, V. P. Fedin, *J. Am. Chem. Soc.* **2012**, *134*, 15640.
- [21] K. Hirata, A. Matsuda, T. Hirata, M. Tatsumisago, T. Minami, *J. Sol-Gel Sci. Technol.* **2000**, *17*, 61.
- [22] Y. Sone, P. Ekdunge, D. Simonsson, *J. Electrochem. Soc.* **1996**, *143*, 1254.
- [23] G. Alberti, M. Casciola, *Solid State Ionics* **2001**, *145*, 3.
- [24] T. Yamada, K. Otsubo, R. Makiura, H. Kitagawa, *Chem. Soc. Rev.* **2013**, *42*, 6655.
- [25] a) N. T. Nguyen, H. Furukawa, F. Gándara, C. A. Trickett, H. M. Jeong, K. E. Cordova, O. M. Yaghi, *J. Am. Chem. Soc.* **2015**, *137*, 15394; b) L. Qin, Y. Z. Yu, P. Q. Liao, W. Xue, Z. Zheng, X. M. Chen, Y. Z. Zheng, *Adv. Mater.* **2016**, *28*, 10772.
- [26] J. Soto-Rodríguez, Z. Hemmatian, E. E. Josberger, M. Rolandi, F. Baneyx, *Adv. Mater.* **2016**, *28*, 6581.
- [27] G. C. Maiti, F. Freund, *J. Chem. Soc. Dalton Trans.* **1981**, *4*, 949.